

# Visualizing kinetic pathways of homogeneous nucleation in colloidal crystallization

Peng Tan<sup>1</sup>, Ning Xu<sup>2</sup> and Lei Xu<sup>1\*</sup>

1. *Department of Physics, The Chinese University of Hong Kong, Hong Kong, China*

2. *Department of Physics, Hefei National*

*Laboratory for Physical Sciences at the Microscale,*

*and CAS Key Laboratory of Soft Matter Chemistry,*

*University of Science and Technology of China, Hefei, China*

(Dated: July 9, 2018)

## Abstract

When a system undergoes a transition from a liquid to a solid phase, it passes through multiple intermediate structures before reaching the final state. However, our knowledge on the exact pathways of this process is limited, mainly due to the difficulty of realizing direct observations. Here, we experimentally study the evolution of symmetry and density for various colloidal systems during liquid-to-solid phase transitions, and visualize kinetic pathways with single-particle resolution. We observe the formation of relatively-ordered precursor structures with different symmetries, which then convert into metastable solids. During this conversion, two major cross-symmetry pathways always occur, regardless of the final state and the interaction potential. In addition, we find a broad decoupling of density variation and symmetry development, and discover that nucleation rarely starts from the densest regions. These findings hold for all our samples, suggesting the possibility of finding a unified picture for the complex crystallization kinetics in colloidal systems.

## Introduction

Crystallization is an important process in condensed matter physics and materials science. As liquid changes into solid, evolutions in both symmetry and density take place. However, the exact kinetic pathways across the liquid-to-solid transition remain as a focus of debate, with no unified picture up to date. Although the classical nucleation theory (CNT) provides a nice framework for understanding crystallization, it has been well recognized that it does not properly describe all aspects of the nucleation process. In the CNT description, the crystallization kinetics proceeds as nucleation and growth of nuclei: small crystals, which have the same symmetry and density as the stable solid, directly emerge from liquid through spontaneous density fluctuation. By contrast, however, previous studies find rather different results: multiple metastable solids that may differ from the stable solid are observed, with one dominant component prevailing in the nucleation process [1, 2]. More specifically, the body-centered cubic (BCC) symmetry dominates the early crystallization in Lennard-Jones and other soft-potential systems [3–8]; while the random hexagonal close-packed (RHCP) structure makes the dominant metastable solid in hard-sphere systems [9–13] (RHCP is a mixture of face-centered cubic (FCC) and hexagonal close-packed (HCP) structures). The kinetic origin of these metastable solids, especially of the dominant component, is currently an outstanding issue requiring experimental elucidation.

Correspondingly, the density variation accompanying such symmetry transformation remains unclear. The traditional view of CNT indicates a simultaneous density and symmetry variation within one step; while recent simulations suggest the possibility of either a two-step variation where densification precedes order construction [14], or a gradual transition in both symmetry and density driven by the bond order fluctuation [15, 16]. The exact density-symmetry correlation depends on the kinetic transformations among different intermediate structures which can be best clarified with single-particle level experiments.

The missing of kinetic information also prevents a clear understanding on the liquid state immediately before crystallization. Unlike the conventional picture of a uniformly disordered liquid state, numerical simulations suggest the existence of relatively-dense or relatively-ordered liquid structures serving as precursors of nuclei [14–20], which may account for an intermediate crystallization step [21–24]. However, the entire picture is far from clear. How does liquid pass through the precursor state to become metastable solids remains a big mystery – even the direct observation of precursors in three-dimensional (3D) real space is

still missing. To tackle this mystery, illustrating the crystallization kinetics again plays an essential role.

In this study, we report single-particle level measurements on the kinetics of 3D colloidal crystallization, for both symmetry and density transformations. To dig out the universal kinetics, extensive studies across different final states and interaction potentials are performed. Colloidal systems are used due to their similar phase-transition behaviors as atomic and molecular systems, while their large particle sizes enabling single-particle level visualization [12, 25–32]. We directly observe relatively-ordered liquid structures behaving as precursors, out of which small nuclei emerge. These precursors exhibit local orders close to HCP, BCC and FCC symmetries, and subsequently convert into these metastable solids. During this precursor-to-solid conversion, interestingly, two major cross-symmetry pathways are universally observed: (1) HCP-like precursors to BCC metastable solid and (2) HCP-like precursors to FCC metastable solid. These major pathways could explain the kinetic origin of the dominant metastable solid. In the density evolution, we surprisingly discover a strong decoupling between density variation and symmetry development, and demonstrate that initial nucleation rarely starts from the densest regions of our samples.

Our system is made up of poly(methyl methacrylate) colloids with diameter  $\sigma = 2.2\mu\text{m}$  and polydispersity less than 2.5%, suspended in a density and refractive index matched solvent. The particles carry charges and form Wigner crystals at low concentrations [33, 34]. We fix the sample concentration at 17% which avoids particle-particle contact and ensures soft-repulsive potential (see “Methods”). By tuning the Debye screening length,  $\kappa^{-1}$ , and the surface charge,  $Z$ , we can obtain BCC-stable and FCC-stable crystals respectively [33, 35]. The phase diagram is shown in the Supplementary Information (SI, Fig.SI-1A). The adjustable stable states offer the opportunity to study kinetic pathways for various transition situations. We shear melt colloidal crystals and record the re-crystallization process immediately after agitation, at the supercooling of  $\Delta T = T_m - T = 0.2T_m \sim 0.4T_m$ , with  $T_m$  being the melting temperature (see “Methods”).

### Three symmetries in precursors and nuclei

By inspecting the local bond order parameters (shown later), we can specify highly-ordered nuclei particles and relatively-ordered liquid particles (in comparison to normal liquid particles), as shown respectively by the dark-brown and light-brown spheres in Fig.1A-C (movie

S1): at the beginning of nucleation in Fig.1A, small nuclei (dark brown) emerge from relatively-ordered liquid structures (light brown) which serve as *precursors* of solid. Moreover, such precursors are continuously created in the subsequent development, as demonstrated by Fig.1B around the stage of critical nuclei size and Fig.1C for the post-critical stage. Precursors wrap the nuclei like a layer of coating and account for an intermediate step in the liquid-solid transition [14–17, 19, 20].

To characterize the local order of any particle  $i$ , we measure its local bond order parameters,  $q_l(i) = (\frac{4\pi}{2l+1} \sum_{m=-l}^{m=l} |q_{l,m}(i)|^2)^{1/2}$ ,  $W_l(i) = \sum_{m_1, m_2, m_3=0}^l \binom{l}{m_1} \binom{l}{m_2} \binom{l}{m_3} \frac{q_{l,m_1}(i)q_{l,m_2}(i)q_{l,m_3}(i)}{|q_l(i)|^3}$ , and the coarse grained bond order parameters,  $\bar{q}_l(i) = (\frac{4\pi}{2l+1} \sum_{m=-l}^{m=l} |\bar{q}_{l,m}(i)|^2)^{1/2}$  (see SI for more information) [36–38]. Good statistics is obtained by locating over  $2 \times 10^6$  particles at 50 different regions within the same sample, in the early crystallization stage (solid fraction  $\sim 5\%$ ). A clear distinction between nuclei and liquid is demonstrated by the number distribution of all particles in the  $\bar{q}_6$ - $\bar{q}_4$  plane in Fig.1D: the upper group with larger  $\bar{q}_6$  is composed by nuclei particles; while the lower group with smaller  $\bar{q}_6$  is by liquid particles. Within the liquid group, we further pick out the particles with relatively high bond order,  $\bar{q}_6 > 0.27$ , as the light-brown precursors shown in Fig.1A-C. According to the two-step nucleation theory, precursors are dense structures with a symmetry lower than solid [17, 18, 20, 22]. Our precursors are therefore defined as the particles with relatively high local order ( $\bar{q}_6 > 0.27$ ) but below the level of solid structures (solid bond number  $\xi < 7$  [37]), in agreement with Kawasaki *et al* [15]. With this definition ( $\bar{q}_6 > 0.27$  and  $\xi < 7$ ), the precursors also have densities higher than normal liquid (see Fig.SI-4D in SI), which is consistent with previous simulations [17, 18, 20, 22]. Note that we can further vary the threshold value of 0.27 to numbers between 0.27 to 0.30, and obtain qualitatively similar results, confirming that the precursor properties do not depend on the choice of exact threshold values.

Several crystalline symmetries appear as we further analyze the local order of nuclei and precursors. For nuclei, three distinct symmetries – BCC, HCP, and FCC – are illustrated by the  $W_4$ - $q_4$  plot in Fig.1E. Clearly, nuclei at the early stage are composed by various components [12], which evolve into one stable solid during much later development. Moreover, the same analysis on precursors reveals this symmetry differentiation even before the solid formation: there exist BCC-like, HCP-like and FCC-like precursors whose local structures are similar to the corresponding nuclei, as shown in Fig.1F and Fig.SI-4C. For the first time,

the experiment reveals multiple symmetries emerging in precursors within the liquid stage, which behave as the “seeds” of the multiple metastable solids and thus account for their kinetic origins.

To verify our symmetry analysis, we plot the radial distribution function,  $g(r)$ , for the three types of nuclei symmetries in Fig.1G: all peaks match precisely with the ideal crystals, confirming the validity of our bond order analysis (note that HCP and FCC have similar  $g(r)$  as expected). Moreover, we find a good match in the main peaks between the precursors (Fig.1H) and the corresponding nuclei (Fig.1G), confirming their underlying structural connection. Because of this structural similarity, the existence of precursors at the liquid-solid interface may dramatically reduce the interfacial tension and promote the rate of nucleation[12, 15]. A small surface tension is also consistent with the ramified nuclei profile observed in the early crystallization stage both in this experiment (see Fig.1A and Fig.1B as an example) and in the previous study [12].

In addition, we clarify one important point: the local order in precursors revealed by us is quite short-ranged, typically extending only to the first shell (the central particle plus its neighbors). When longer ranges are involved, however, the bulk phase of precursor clusters is quite amorphous, due to the mixing and interfering of multiple components (see Fig.2A). In comparison to the previous studies, our precursor definition is similar to the one by Kawasaki *et al* [15]; but is probably only part of the precursors defined in some other studies [17, 18, 20, 22], which may also contain a truly amorphous fraction. To study this truly amorphous fraction, dynamic investigations regarding the lifetime of dense amorphous clusters would be needed. In conclusion, the precursors in our study exhibit multiple local orders at short-range, but are amorphous at intermediate and long ranges (see more details in SI, session IIC, page 10-15).

**Kinetic pathways during precursor-to-solid conversion**

Our experiment confirms the existence of precursors, which exhibit various symmetries and convert into different metastable solids. However, the symmetry transformation during the precursor-to-solid conversion requires further illumination. To visualize the process, we color the three symmetries differently and demonstrate their evolutions in Fig.2A-C (movie S2): at the very beginning in Fig.2A, the HCP symmetry (nuclei + precursors, purple spheres) dominates the other two, while the BCC symmetry (red spheres) catches up around the

critical nuclei size in Fig.2B, and later dominates the system (see Fig.2C). This particular sample eventually develops into a BCC crystal.

The system evolves from HCP-dominant to BCC-dominant, indicating transformations across different symmetries. To figure out the transformation pathways, we track the relative fractions of different symmetries with respect to time, for both precursors and nuclei. The typical result for a BCC-stable system is demonstrated in Fig.2D: for all three symmetries, the precursor (open symbols) and nuclei (close symbols) curves are roughly parallel, demonstrating their close correlation. However, a gap also exists between the two, revealing cross-symmetry transformations during the precursor-to-solid conversion. More specifically, in the HCP panel the precursor curve is higher than the nuclei one, indicating an extra fraction of HCP-like precursors that must convert into other types of nuclei. Correspondingly, in BCC and FCC panels excess fractions of nuclei (instead of precursors) are found, reconfirming the conversion from HCP-like precursors. Therefore our data indicate two cross-symmetry pathways during the precursor-to-solid conversion: (1) HCP-like precursors to BCC nuclei and (2) HCP-like precursors to FCC nuclei. The same kinetic pathways are also observed in a typical FCC-stable system, as shown in Fig.2E. In addition, hard-sphere systems exhibit the same behavior (see Fig.SI-12 in SI) as well, demonstrating the general validity of the two cross-symmetry pathways.

To visualize the pathways directly, we illustrate all possible conversions between different types of precursors and nuclei in the  $\bar{q}_6 - q_4$  plane in Fig.2F: the  $\bar{q}_6$  values are used for distinguishing nuclei from precursors; while the  $q_4$  values are used for distinguishing different symmetries. The lower cluster indicates precursors, the upper cluster represents nuclei, and the connection in between is from the particles caught during the precursor-to-nuclei conversion which directly visualizes the kinetic pathway. Clearly, a pathway always exists for a conversion within the same symmetry as demonstrated by the three corresponding images in Fig.2F (upper-left to lower-right diagonal), which verifies the previous simulation [16]. More interestingly, cross-symmetry pathways previously never reported also appear. Two strong pathways from HCP-precursors to BCC-nuclei and FCC-nuclei are revealed in the second row, consistent with Fig.2D and Fig.2E. At the same time, two weak pathways from BCC-precursors and FCC-precursors to HCP-nuclei are also found, although overwhelmed by the effect from the two strong ones just mentioned. For the interaction between BCC and FCC symmetries, there is essentially no pathway during the conversion. These kinetic

pathways are universally observed in all our soft-repulsive systems.

In soft-repulsive systems, we observe dominant HCP-like precursors initially [15, 16], which can subsequently convert into BCC and FCC nuclei via two cross-symmetry pathways. However, the pathway to BCC-nuclei is much more significant, as demonstrated by its much stronger magnitude (see Fig.2F, 2nd row, the leftmost image compared with the rightmost image). Correspondingly, BCC-symmetry dominates the early metastable solid phase in both our soft-repulsive samples and the systems previously studied [2–7]. Therefore, we propose that the dominant cross-symmetry pathway probably leads to the dominant metastable solid in early crystallization. To further test this scenario, we perform the same measurements in hard-sphere systems, whose dominant metastable solid is RHCP (mixture of FCC and HCP) instead of BCC [12, 13]. As expected, the dominant pathway changes accordingly: the HCP-like precursors now mainly transfer into FCC-nuclei instead of BCC, as FCC is one important component of the RHCP structure (see Fig.SI-12 in SI). Both the soft-repulsive and hard-sphere experiments are consistent with our newly proposed scenario, which explains the kinetic origin of the *dominant* metastable solid in early crystallization.

We summarize our crystallization kinetics in Fig.2G. As temperature drops below the melting point, precursors emerge out of liquid, with the HCP-like component dominating the BCC-like and the FCC-like ones. These precursors then convert into metastable solids. Besides the conversion within the same symmetry, interestingly, cross-symmetry pathways also exist: there are two major ones from HCP-like precursors to BCC and FCC nuclei, and two minor ones from BCC-like and FCC-like precursors to HCP nuclei, as represented by the solid and dashed lines respectively. The effect of major pathways overwhelm the effect of minor ones. Eventually all metastable solids evolve into the stable solid [39].

### Density-symmetry correlation

In the process of crystallization, the establishment of crystalline order is naturally accompanied by density change. We illustrate their correlation by directly measuring the variation of local density with respect to the development of local order. The local density,  $\rho$ , is determined by the Voronoi diagram; and the local order is quantified by the solid bond number,  $\xi$  (see SI for the exact definition). Typically a larger  $\xi$  indicates a better crystalline order. Good statistics is obtained from measurements over  $10^6$  particles in the early crystallization stage (solid fraction  $\sim 5\%$ ). At each solid bond number, we obtain the average local density

and illustrate their correlation in the  $\rho$ - $\xi$  plot.

A typical  $\rho$ - $\xi$  dependence is shown by the solid symbols in Fig.3A for a BCC-stable system. Clearly there exists a density plateau over a broad range of local order,  $3 \leq \xi \leq 10$ , indicating very little density change against a significant development of order. In particular, across the hatched area of liquid-solid boundary ( $6 \leq \xi \leq 8$ ),  $\rho$  does not experience any abrupt increase, in sharp contrast to the density jump described in the classical nucleation theory. Significant densification only occurs at either quite early ( $\xi < 3$ ) or rather late ( $\xi > 10$ ) stages of local order construction, and corresponds respectively to the initial formation of precursors and the final perfection of local order. We note that particles with  $3 \leq \xi \leq 6$  largely overlap with the precursor particles defined previously (see their similar  $g(r)$  in Fig.SI-6). Consequently, our experiment reveals a rather complex three-stage correlation for density and symmetry development: initially they grow simultaneously during the formation of precursors ( $\xi < 3$ ), followed by a decoupling plateau throughout precursor-to-solid conversion ( $3 \leq \xi \leq 10$ ), and then reappears the simultaneous growth for the final perfection of local order ( $\xi > 10$ ). This three-stage trend has never been reported previously and requires further theoretical explanation.

Different symmetries and structures emerge as early as in the liquid stage, and therefore we illustrate their density variations separately as well. We can divide the densities of most particles ( $> 98\%$ ) into two branches: the 14-neighbor branch (BCC-like) and the 12-neighbor branch (FCC-like and HCP-like), as shown by the open symbols in Fig.3A. The two branches exhibit a large difference at low  $\xi$ , which diminishes as crystalline order increases. Moreover, before the order is fully constructed, the 14-neighbor branch is always below the 12-neighbor one, indicating a lower density for the BCC-like structure. Since we observe a major pathway from HCP-like precursors to BCC nuclei in the soft-repulsive systems, it indicates a conversion from the high-density branch to the low-density one. This conversion apparently lowers the high-density branch, raises the low-density one, while keeps the average density largely unchanged, as revealed by the plateau of solid symbols. Similar results are also observed in the FCC-stable systems shown in Fig.3B, except with two minor differences: (1) there is a sharper density increase after the plateau, and (2) the fully developed FCC crystal (i.e., the end point of upper branch) is denser than the BCC counterpart (i.e., the end point of lower branch) while the opposite is true in Fig.3A.

Over a broad range of order construction, a decoupling plateau between density variation



and symmetry development is observed, especially at the liquid-to-solid transition boundary ( $6 \leq \xi \leq 8$ ). Such discrepancy with the classical picture is even more apparent when we compare the spatial distributions of  $\xi$  and  $\rho$  in the early crystallization stage: very little correlation is found between the nucleation events indicated by  $\xi$  in Fig.3C and the dense regions specified by  $\rho$  in Fig.3D. The densest regions ( $\rho > 1.02$ , orange areas) are significantly denser than the nuclei ( $\rho \sim 1.01$ ), and appear mostly at disordered locations. At the same time, the local density fluctuations in both space and time are more than 5%, much larger than the density mismatch between liquid and nuclei (1%  $\sim$  2%). To further test this result, we plot the spatial distribution of local bond order,  $\bar{q}_6$ , in Fig.3E, and again find very little correlation with the density plot in Fig.3D. These results unambiguously demonstrate that nucleation events *do not* start from the densest regions, in sharp contrast to the conventional picture of nucleation. However, the similarity between Fig.3C and Fig.3E indicates a strong correlation between the nucleation events and the local bond order[15, 16].

## Discussions

One important question remains unclear: why the HCP-like precursors dominate initially? We believe it is due to the common feature of tetrahedra clusters adjacent by faces, which widely appear in both the disordered liquid [40] and the HCP-like precursors. This structural similarity makes the transformation to HCP-like precursors a major first step. Subsequently, the local HCP-like symmetry converts into other symmetries via slight deformations: a shear parallel to the hexagonal plane can result in FCC symmetry while an in-plane compression (or stretch) may lead to BCC structure. Both approaches only involve locally small movements with little energy cost, while they produce significant changes in symmetry. The underlying inhomogeneous stresses may come from the surface tension of ramified liquid-solid interfaces, as supported by the observation that symmetry conversion mainly occurs at this interface. However this picture is largely qualitative and calls for further study.

Moreover, the density fluctuations at single particle level exceed the liquid-solid density mismatch substantially, implying that local structures can easily fluctuate in and out of the solid density. Combining with the observation that nucleation rarely starts from the densest regions, we suspect that density fluctuation may not be the main driving factor for our crystallization process; instead the local bond order fluctuation could be a reasonable candidate[16]. Illustrating these emerging questions should shed new light on the conven-

tional picture of crystallization.

## methods

Our system is made up of NBD dyed poly(methyl methacrylate) (PMMA) colloids with diameter  $\sigma = 2.2\mu\text{m}$  and polydispersity less than 2.5%. The colloids are suspended in a mixture of non-polar and weakly-polar solvents, which closely matches both the refractive index and the density of particles (see Experimental Details and Phase Diagram in the Supplementary Information (SI) for more details). The particles are charge-stabilized in the solvent, with the weakly-screened electric repulsion causing Wigner crystals at low concentrations [33, 34]. To ensure soft-repulsive interaction, we fix the concentration of all samples at 17% which avoids direct contacts among particles. By adjusting the volume ratio between the non-polar to weakly-polar solvents [33], we can tune the Debye screening length,  $\kappa^{-1}$ , and the surface charge,  $Z$  [35]. This leads to different stable solid states: at long screening lengths, the BCC symmetry is most stable; while at short screening lengths, the most stable symmetry becomes FCC. We measure the phase diagram with various samples (see Fig.SI-1A in SI), and show the detailed analysis of two typical samples, BCC-stable ( $\kappa^{-1} \sim 960$  nm) and FCC-stable ( $\kappa^{-1} \sim 520$  nm), respectively. The adjustable stable states offer the opportunity to study various precursor-to-solid(metastable) kinetic pathways. We shear melt colloidal crystals and record the re-crystallization process immediately after agitation, with a Leica Sp5 confocal microscope scanning in three dimensions with respect to time. We can estimate the degree of supercooling below the melting temperature,  $\Delta T = T_m - T$ , for all our solid samples in the phase diagram. Two different approaches are applied: the distance from the melting line yields  $\Delta T = 0.2T_m \sim 0.44T_m$ ; and the Lindemann parameter approach [41, 42] gives  $\Delta T = 0.2T_m \sim 0.4T_m$ . The two independent estimates agree with each other within the experimental accuracy.

**Correspondence and requests:** Correspondence and requests for materials should be addressed to L. X.

**Acknowledgements:** P. T. and L. X. are supported by the Research Grants Council of Hong Kong (GRF grant CUHK404211, ECS grant CUHK404912, CUHK Direct Grant 4053021), and N. X. is supported by National Natural Science Foundation of China (No. 91027001 and 11074228), National Basic Research Program of China (973 Program No. 2012CB821500), CAS 100-Talent Program (No. 2030020004), and Fundamental Research Funds for the Central Universities (No. 2340000034). We thank Hajime Tanaka and Eli

Sloutskin for helpful discussions, and Andrew Schofield for providing the particles.

**Author contributions:** P. T. and L. X. conceived and designed the experiments, P. T. performed the experiments, P. T., N. X. and L. X. analyzed the data, P. T. developed the new approach of local bond order analysis, P. T. and L. X. wrote the paper.

- 
- [1] Ostwald, W. Studien über die Bildung und Umwandlung fester Körper. 1. Abhandlung: Übersättigung und Überkaltung, *Z. Phys. Chem.* **22**, 289-330 (1897).
  - [2] Alexander, S. & McTague, J. Should All Crystals Be bcc? Landau Theory of Solidification and Crystal Nucleation, *Phys. Rev. Lett.* **41**, 702-705 (1978).
  - [3] ten Wolde, P. R., Ruiz-Montero, M. J. & Frenkel, D. Numerical Evidence for bcc Ordering at the Surface of a Critical fcc Nucleus, *Phys. Rev. Lett.* **75**, 2714-2717 (1995).
  - [4] ten Wolde, P. R., Ruiz-Montero, M. J. & Frenkel, D. Numerical calculation of the rate of crystal nucleation in a Lennard-Jones system at moderate undercooling, *J. Chem. Phys.* **104**, 9932-9947 (1996).
  - [5] Shen, Y. C. & Oxtoby, D. W. bcc Symmetry in the Crystal-Melt Interface of Lennard-Jones Fluids Examined through Density Functional Theory, *Phys. Rev. Lett.* **77**, 3585-3588 (1996).
  - [6] Auer, S. & Frenkel, D. Crystallization of weakly charged colloidal spheres: a numerical study, *J. Phys.: Condens. Matter* **14**, 7667 (2002).
  - [7] Moroni, D., ten Wolde, P. R., & Bolhuis, P. G. Interplay between Structure and Size in a Critical Crystal Nucleus, *Phys. Rev. Lett.* **94**, 235703 (2005).
  - [8] Russo, J. & Tanaka, H. Selection mechanism of polymorphs in the crystal nucleation of the Gaussian core model, *Soft Matter* **8**, 4206-4215 (2012).
  - [9] Pusey, P. N. & van Megen, W. Phase behaviour of concentrated suspensions of nearly hard colloidal spheres, *Nature* **320**, 340-342 (1986).
  - [10] Pusey, P. N. *et al.* Structure of crystals of hard colloidal spheres, *Phys. Rev. Lett.* **63**, 2753-2756 (1989).
  - [11] Zhu, J. *et al.* Crystallization of hard-sphere colloids in microgravity, *Nature* **387**, 883-885 (1997).
  - [12] Gasser, U., Weeks, E. R., Schofield, A., Pusey, P. N. & Weitz, D. A. Real-Space Imaging of Nucleation and Growth in Colloidal Crystallization, *Science* **292**, 258-262 (2001).

- [13] Auer, S. & Frenkel, D. Prediction of absolute crystal-nucleation rate in hard-sphere colloids, *Nature* **409**, 1020-1023 (2001).
- [14] tenWolde, P. R. & Frenkel, D. Enhancement of Protein Crystal Nucleation by Critical Density Fluctuations, *Science* **277**, 1975-1978 (1997).
- [15] Kawasaki, T. & Tanaka, H. Formation of a crystal nucleus from liquid, *Proc. Nat. Acad. Sci.* **107**, 14036-14041 (2010).
- [16] Russo, J. & Tanaka, H. The microscopic pathway to crystallization in supercooled liquids, *Scientific Reports* **2**, 505 (2012).
- [17] Schilling, T., Schöpe, H. J., Oettel, M., Opletal, G. & Snook, I. Precursor-Mediated Crystallization Process in Suspensions of Hard Spheres, *Phys. Rev. Lett.* **105**, 25701(2010).
- [18] Tóth, G. I., Pusztai, T., Tegze, G., Tóth, G., & Gránásy, L. Amorphous Nucleation Precursor in Highly Nonequilibrium Fluids, *Phys. Rev. Lett.* **107**, 175702 (2011).
- [19] Lechner, W., Dellago, C. & Bolhuis, P. G. Role of the Prestructured Surface Cloud in Crystal Nucleation, *Phys. Rev. Lett.* **106**, 85701 (2011).
- [20] Lutsko, J. F. & Nicolis, G. Theoretical Evidence for a Dense Fluid Precursor to Crystallization, *Phys. Rev. Lett.* **96**, 046102 (2006).
- [21] Martin, S., Bryant, G. & van Meegen, W. Crystallization kinetics of polydisperse colloidal hard spheres: Experimental evidence for local fractionation, *Phys. Rev. E* **67**, 061405 (2003).
- [22] Schöpe, H. J., Bryant, G. & van Meegen, W. Two-Step Crystallization Kinetics in Colloidal Hard-Sphere Systems, *Phys. Rev. Lett.* **96**, 175701 (2006).
- [23] Iacopini, S., Palberg, T. & Schöpe, H. J. Crystallization kinetics of polydisperse hard-sphere-like microgel colloids: Ripening dominated crystal growth above melting, *J. Chem. Phys.* **130**, 084502 (2009).
- [24] Savage, J. R. & Dinsmore, A. D. Experimental Evidence for Two-Step Nucleation in Colloidal Crystallization, *Phys. Rev. Lett.* **102**, 198302 (2009).
- [25] Larsen, A. E. & Grier, D. G. Like-charge attractions in metastable colloidal crystallites, *Nature* **385**, 230-233 (1997).
- [26] Weeks, E. R., Crocker, J. C., Levitt, A. C., Schofield, A. & Weitz, D. A. Three-Dimensional Direct Imaging of Structural Relaxation Near the Colloidal Glass Transition, *Science* **287**, 627-631 (2000).
- [27] Anderson, V. J. & Lekkerkerker, H. N. Insights into phase transition kinetics from colloid

- science, *Nature* **416**, 811-815 (2002).
- [28] Schall, P., Cohen, I., Weitz, D. A. & Spaepen, F. Visualization of Dislocation Dynamics in Colloidal Crystals, *Science* **305**, 1944-1948 (2004).
- [29] Alsayed, A. M., Islam, M. F., Zhang, J., Collings, P. J. & Yodh, A. G. Premelting at Defects Within Bulk Colloidal Crystals, *Science* **309**, 1207-1210 (2005).
- [30] Savage, J. R., Blair, D. W., Levine, A. J., Guyer, R. A. & Dinsmore, A. D. Imaging the Sublimation Dynamics of Colloidal Crystallites, *Science* **314**, 795-798 (2006).
- [31] Lu, P. J., Zaccarelli, E., Ciulla, F., Schofield, A. B., Sciortino, F. & Weitz, D. A. Gelation of particles with short-range attraction, *Nature* **453**, 499-503 (2008).
- [32] Wang, Z. R., Wang, F., Peng, Y., Zheng, Z. Y. & Han, Y. L. Imaging the Homogeneous Nucleation During the Melting of Superheated Colloidal Crystals, *Science* **338**, 87-90 (2012).
- [33] Leunissen, M. E. *et al.* Ionic colloidal crystals of oppositely charged particles, *Nature* **437**, 235-240 (2005).
- [34] Tan, P., Xu, N., Schofield, A. & Xu, L. Understanding the Low-Frequency Quasilocalized Modes in Disordered Colloidal Systems, *Phys. Rev. Lett.* **108**, 095501 (2012).
- [35] Hynninen, A. & Dijkstra, M. Phase diagrams of hard-core repulsive Yukawa particles, *Phys. Rev. E* **68**, 021407 (2003).
- [36] Steinhardt, P. J., Nelson, D. R. & Ronchetti, M. Bond-orientational order in liquids and glasses, *Phys. Rev. B* **28**, 784-805 (1983).
- [37] ten Wolde, P., Ruiz-Montero, M. J. & Frenkel, D. Simulation of homogeneous crystal nucleation close to coexistence, *Faraday Discuss* **104**, 93-110 (1996).
- [38] Lechner, W. & Dellago, C. Crystal structures based on averaged local bond order parameters, *J. Chem. Phys.* **129**, 114707 (2008).
- [39] We find the dominant solid phase in our experiments is BCC( $\lambda \sim 960$  nm) or RHCP( $\lambda \sim 520$  nm) after several days.
- [40] Anikeenko, A. V. & Medvedev, N. N. Polytetrahedral Nature of the Dense Disordered Packings of Hard Spheres, *Phys. Rev. Lett.* **98**, 235504 (2007).
- [41] Meijer, E. J. & Frenkel, D. Melting line of Yukawa system by computer simulation, *J. Chem. Phys.* **94**, 2269-2271 (1991).
- [42] Zahn, K. & Maret, G. Dynamic Criteria for Melting in Two Dimensions, *Phys. Rev. Lett.* **85**, 3656-3659 (2000).

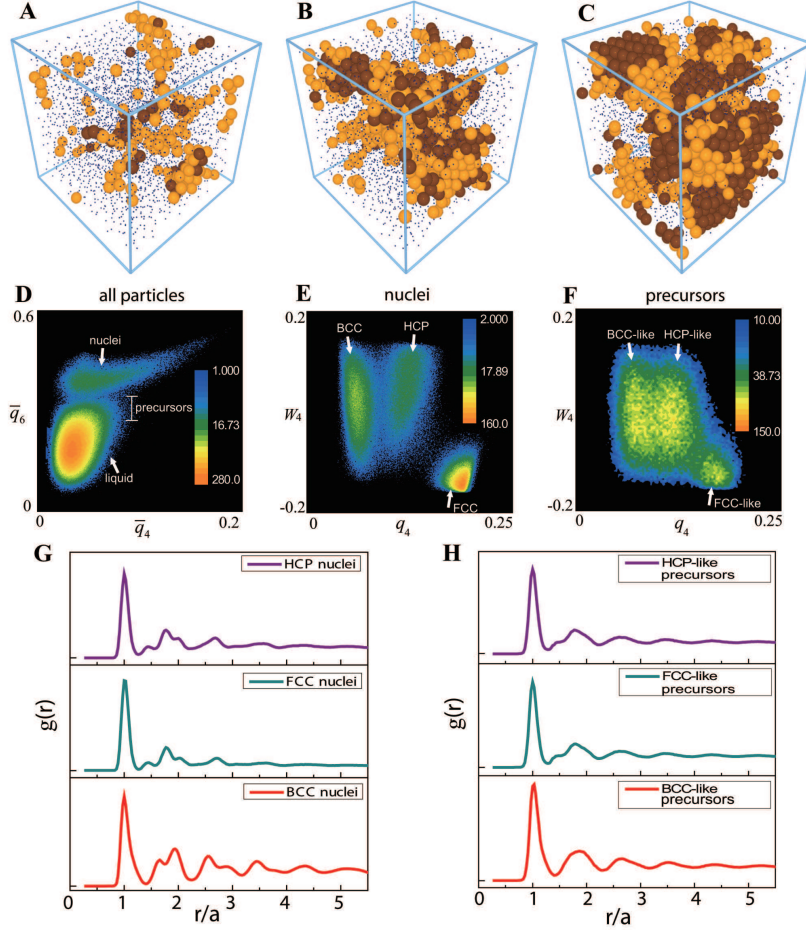


FIG. 1: **Structures of nuclei and precursors in early crystallization.** **A-C**, precursor mediated crystallization in a BCC-stable ( $\kappa^{-1} = 960\text{nm}$ ) system. The dark-brown spheres represent nuclei particles while the light-brown ones indicate relatively-ordered liquid particles we define as precursors. The blue dots are normal liquid particles. At the beginning of nucleation (**A**,  $\phi_{nuclei} = 1.9\%$ ,  $\phi_{precursor} = 5.6\%$ ,  $t = 240\text{s}$ ), nuclei embryos emerge from clusters of precursors. During the subsequent development around critical (**B**,  $\phi_{nuclei} = 7.1\%$ ,  $\phi_{precursor} = 11.6\%$ ,  $t = 2640\text{s}$ ) and post-critical (**C**,  $\phi_{nuclei} = 21.4\%$ ,  $\phi_{precursor} = 20.4\%$ ,  $t=6480\text{s}$ ) nuclei sizes, precursors are continuously created around nuclei. **D**, number distribution of all particles in the  $\bar{q}_6 - \bar{q}_4$  plane in the early crystallization (solid fraction  $\sim 5\%$ ). The upper group with higher  $\bar{q}_6$  is composed by nuclei particles; and the lower group is composed by liquid particles. Within the liquid group, relatively-ordered particles with  $\bar{q}_6 > 0.27$  are defined as precursors. **E**, number distribution of nuclei in the  $W_4-q_4$  plane reveals three meta-stable crystalline symmetries: BCC, HCP and FCC. **F**,  $W_4-q_4$  plot of precursors reveals BCC-like, HCP-like and FCC-like precursors in the liquid stage. **G** and **H**, radial distribution function for the three types of nuclei and precursor symmetries.  $r$  is re-normalized by the average particle distance,  $a$ . A good match in the main peaks between **G** and **H** suggests a structural similarity between precursors and nuclei.

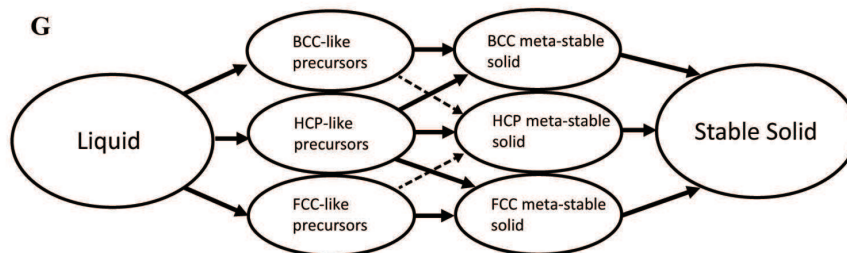
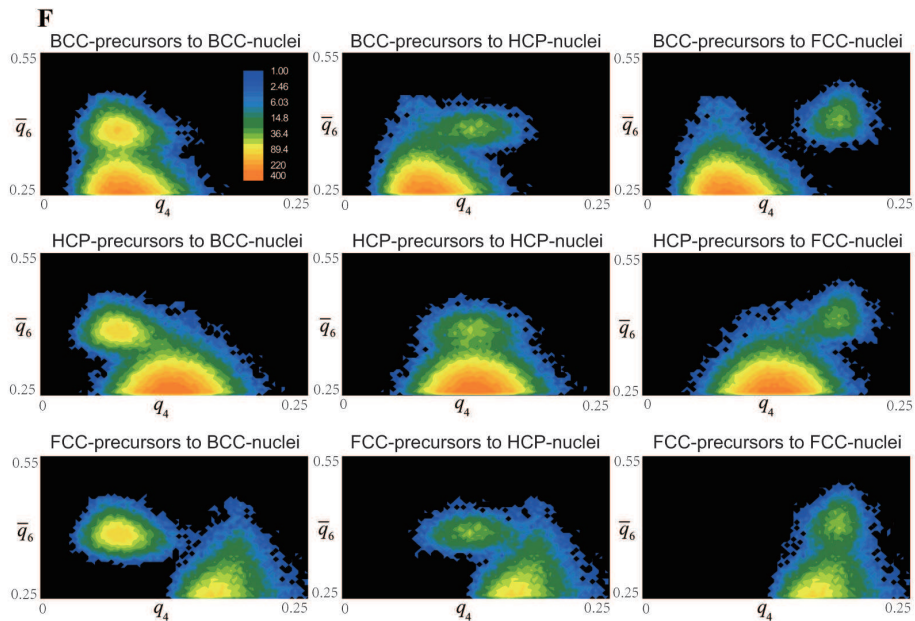
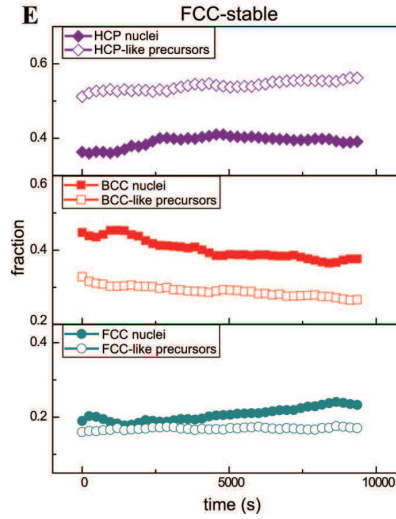
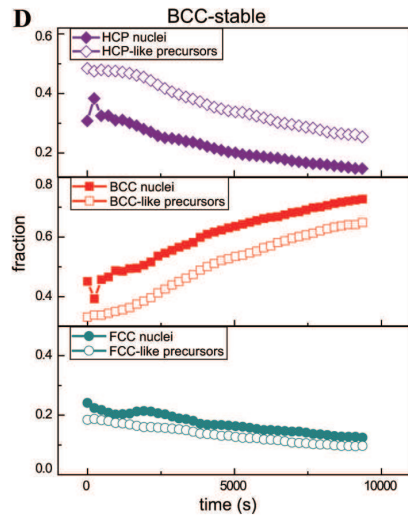
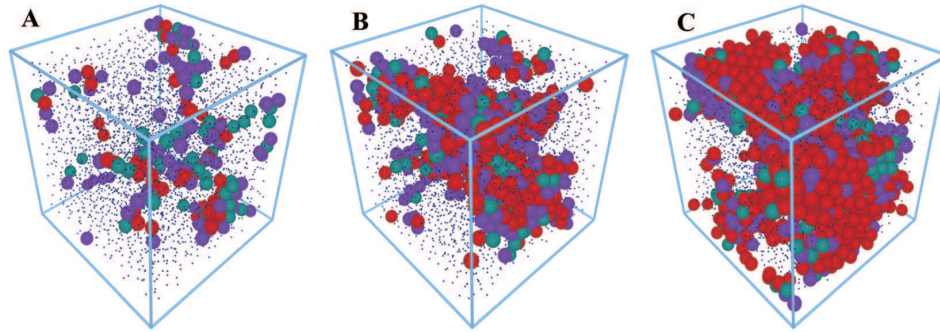
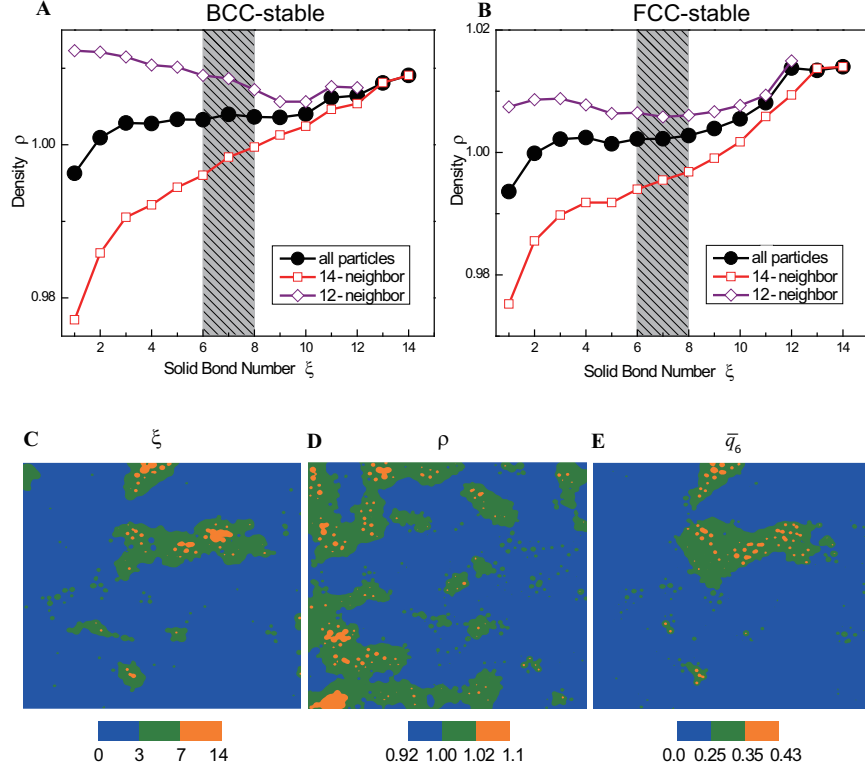


FIG. 2: Fig. 2. **Kinetic pathways during crystallization.** **A-C**, Time evolution of different symmetries. The purple spheres indicate HCP nuclei and HCP-like precursors, the red spheres represent BCC nuclei and BCC-like precursors, and the green spheres demonstrate FCC nuclei and FCC-like precursors. The three instants are identical to the ones in Fig.1A-C. The HCP-symmetry (purple) initially dominates, while the BCC-symmetry (red) takes over afterwards. **D**, relative fractions of precursors (open symbols) and nuclei (close symbols) for every symmetry in a BCC-stable ( $\kappa^{-1} = 960\text{nm}$ ) system. The precursor and nuclei curves are mostly parallel, indicating their strong correlation. In the HCP panel, the precursor curve is above the nuclei one; while in BCC and FCC panels, the precursor curve is below the nuclei one. This indicates two kinetic pathways from the HCP-like precursors to BCC and FCC nuclei. The critical nuclei size is reached around  $t = 2640s$ . **E**, the same pathways are also observed in an FCC-stable ( $\kappa^{-1} = 520\text{nm}$ ) system. The critical nuclei size is reached around  $t = 2400s$ . **F**, direct visualization of kinetic pathways in  $\bar{q}_6 - q_4$  plane. Each image illustrates the conversion from one type of precursors to one type of nuclei. The lower cluster indicates precursors, the upper cluster represents nuclei, and the connection in between visualizes the pathway. For conversions within the same symmetry, a pathway always exists. For cross-symmetry conversions, there are two major pathways from HCP-precursors to BCC and FCC nuclei and two weak pathways from BCC and FCC precursors to HCP-nuclei. There is essentially no pathway between the FCC and BCC symmetries. **G**, summary of kinetics during the precursor-mediated crystallization. Solid lines indicate the major pathways, while dashed lines represent the weak pathways.





**FIG. 3: Local density evolution throughout crystallization.** **A**, the local density,  $\rho$ , versus the solid bond number,  $\xi$ , in a BCC-stable ( $\kappa^{-1} = 960\text{nm}$ ) system. The solid symbols represent the average local density as a function of the local order development. As  $\xi$  increases,  $\rho$  first experiences a rapid increase which corresponds to the precursor formation, followed by a broad plateau ( $3 < \xi < 10$ ) which corresponds to the precursor-to-solid conversion. In particular, no density jump is observed at the hatched area of liquid-solid transition boundary, in sharp contrast to the CNT description. The second increase occurs at  $\xi > 10$  as the local order undergoes the final perfection in nuclei. The open symbols demonstrate the 14-neighbor branch (BCC) and the 12-neighbor branch (HCP and FCC). At low  $\xi$  there exists a large gap between the two branches, which diminishes with the increase of order. Before the order is fully constructed, the 14-neighbor branch is always below the 12-neighbor one, indicating the lower density of BCC structure. However, eventually the 14-bond (BCC) crystal becomes denser than the 12-bond (FCC and HCP) crystal. **B**, the same measurements in an FCC-stable ( $\kappa^{-1} = 520\text{nm}$ ) system. A similar three-stage correlation is observed, but the end point of the 12-neighbor branch is now higher than the end point of the 14-neighbor branch. **C-E**, a snapshot of the spatial distributions for the solid bond number ( $\xi$ ), local density ( $\rho$ ) and the local bond order parameter ( $\bar{q}_6$ ). The data are taken in a  $5\mu\text{m}$  thick slice at the early crystallization stage. Clearly the density plot has a poor correlation with the other two, indicating that the nucleation events (regions with high  $\xi$  and  $\bar{q}_6$  values) rarely start from the densest regions.